A Second Conserved GAF Domain Cysteine Is Required for the Blue/Green Photoreversibility of Cyanobacteriochrome Tlr0924 from *Thermosynechococcus elongatus*[†]

Nathan C. Rockwell,[‡] Stephanie Lane Njuguna,[§] Laurel Roberts,[§] Elenor Castillo,[§] Victoria L. Parson,[§] Sunshine Dwojak,[§] J. Clark Lagarias,*[,‡] and Susan C. Spiller*[,§]

Section of Molecular and Cellular Biology, University of California, Davis, California 95616, and Department of Biology, Mills College, Oakland, California 94613

Received January 16, 2008; Revised Manuscript Received May 19, 2008

ABSTRACT: Phytochromes are widely occurring red/far-red photoreceptors that utilize a linear tetrapyrrole (bilin) chromophore covalently bound within a knotted PAS-GAF domain pair. Cyanobacteria also contain more distant relatives of phytochromes that lack this knot, such as the phytochrome-related cyanobacteriochromes implicated to function as blue/green switchable photoreceptors. In this study, we characterize the cyanobacteriochrome Tlr0924 from the thermophilic cyanobacterium *Thermosynechococcus elongatus*. Full-length Tlr0924 exhibits blue/green photoconversion across a broad range of temperatures, including physiologically relevant temperatures for this organism. Spectroscopic characterization of Tlr0924 demonstrates that its green-absorbing state is in equilibrium with a labile, spectrally distinct blue-absorbing species. The photochemically generated blue-absorbing state is in equilibrium with another species absorbing at longer wavelengths, giving a total of 4 states. Cys499 is essential for this behavior, because mutagenesis of this residue results in red-absorbing mutant biliproteins. Characterization of the $C_{499}D$ mutant protein by absorbance and CD spectroscopy supports the conclusion that its bilin chromophore adopts a similar conformation to the red-light-absorbing P_r form of phytochrome. We propose a model photocycle in which *Z*/*E* photoisomerization of the 15/16 bond modulates formation of a reversible thioether linkage between Cys499 and C10 of the chromophore, providing the basis for the blue/green switching of cyanobacteriochromes.

Photosynthetic organisms face the need to coordinate their metabolic responses to their light environment, so that photosynthesis and redox balance are properly maintained for growth. This is accomplished by a wide range of photosensory proteins (*1, 2*). The first such proteins to be discovered were the phytochromes, which are red/far-red photosensors initially described in plants and later shown to be widespread in both photosynthetic and nonphotosynthetic organisms (*3, 4*). Upon excitation with red light, phytochromes photoconvert from the red-absorbing P_r state[1], which is usually thermally stable, to the far-red absorbing P_{fr} state (*5*). This reversible interconversion is the result of light-driven *Z*/*E* isomerization of the 15/16 double bond of the protein-bound bilin chromophore (Figure 1), which is covalently attached to a Cys residue in the conserved photosensory core of phytochromes. This photosensory core is generally found N-terminal to putative output domains implicated in signal transduction, such as the histidine kinase domain of the cyanobacterial phytochrome Cph1 (*6*). Since both P_r and P_{fr} states can generate signaling outputs (*4, 7*), light modulates the signaling activity of phytochromes.

The photosensory core of phytochromes is composed of three distinct domains: a PAS domain, a GAF domain, and a PHY domain (*3, 4, 8*). Crystal structures are now available for the PAS and GAF domains of two bacterial phytochromes, *Dr*BphP from *Deinococcus radiodurans* and *Rp*BphP3 from *Rhodopseudomonas palustris* (*9–11*). These structures reveal a surprising knotted architecture for the two

[†] This work was supported in part by grants GM068552 (to J.C.L.) and RR008605 (to Pittsburgh Supercomputing Center) from the National Institutes of Health, by subcontracts from the National Science Foundation Center for Biophotonics Science and Technology (PHY-0120999, J.C.L., and 002865-MC, S.C.S.) and by a grant from the National Science Foundation (BES-0304798) to S.C.S.

* Corresponding authors. J.C.L.: tel, 530-752-1865; fax, 530-752-3085; e-mail, jclagarias@ucdavis.edu. S.C.S.: tel, (510) 430-3175; e-mail, spiller@mills.edu.

[‡] University of California.

[§] Mills College.

[1] Abbreviations: α-PC, α subunit of C-phycocyanin, containing a single PCB chromophore; α-PEC, α subunit of C-phycoerythrocyanin, containing a single PVB chromophore; BBP, bilin-binding protein from *Pieris brassicae;* BSA, bovine serum albumin; BV, biliverdin IXα; CD, electronic circular dichroism; eV, electronvolt; *f,* oscillator strength; GAF, domain acronym derived from vertebrate cGMP-specific phosphodiesterases, cyanobacterial adenylate cyclases, and formate hydrogen lyase transcription activator FhlA; λ_{calc}, peak calculated wavelength; λ_{max}, peak observed wavelength for an absorbance band; PAS, domain acronym derived from period clock (PER) protein, aromatic hydrocarbon receptor nuclear translocator (ARNT), and single-minded (SIM); P_b, a blue-absorbing state of Tlr0924 and PixJ; P_b^L, thermally labile blue-absorbing state of Tlr0924; P_b^S, thermally stable blue-absorbing state of Tlr0924; PCB, phycocyanobilin; P_{fr}, phytochrome far-red absorbing state; P_g, green-absorbing state of Tlr0924 and PixJ having peak absorbance at ~538 nm; P_g', green-absorbing state of Tlr0924 having peak absorbance at ~560 nm; P_r, phytochrome red-absorbing state; PVB, phycoviolobilin; SDS, sodium dodecyl sulfate; TDDFT, time-dependent density functional theory.

10.1021/bi800088t CCC: $40.75
Published on Web 06/13/2008

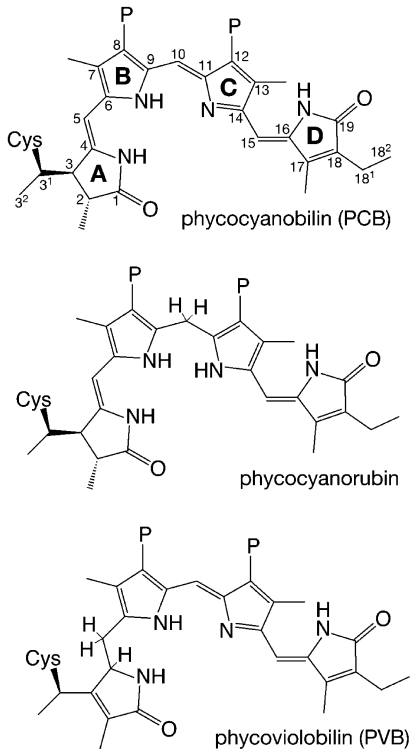

FIGURE 1: Thioether adducts of linear tetrapyrroles. Top, the cyanobacterial phytochrome Cph1 utilizes phycocyanobilin (PCB) as chromophore. Cys259 forms a covalent linkage with the $C3^1$ atom of PCB (*8, 18*). PixJ is known to form a similar covalent linkage to PCB (*24*). Ring designations are indicated in bold, and the numbering for the carbon atoms is indicated. Middle, phycocyanorubin can be produced from PCB by reduction of the C10 position. This can be accomplished enzymatically with isolated PCB (*66*) or can be performed with chemical reductants for denatured phycobiliproteins (*65*). Bottom, α-phycoerythrocyanin (α-PEC) utilizes PCB as chromophore precursor, but PCB is tautomerized to phycoviolobilin (PVB) during the assembly reaction by accessory factors (*79, 80*). The tautomerization of PCB to PVB results in a shorter conjugated system with a blue-shifted spectrum. All compounds are drawn with the *R* stereochemistry at $C3^1$ demonstrated for plant phytochrome (*32*) and are shown in the 5-*Z,syn,* 10-*Z,syn,* 15-*Z,anti* configuration of phytochrome in the P_r state (*9–11*). P, propionate.

domains, with the bilin chromophore bound in a C5-*Z,syn,* C10-*Z,syn,* C15-*Z,anti* configuration (Figure 1) in a pocket within the GAF domain. Conservation of primary sequence elements in these two domains suggests that this architecture will be common to all phytochromes (*9, 12*). By contrast, the precise structure of the bilin chromophore (i.e., biliverdin IXα (BV), phycocyanobilin (PCB), or phytochromobilin), the location of the Cys residue ligated to the bilin, and the nature of that linkage have diverged during the evolution of this photoreceptor family (*7, 10*). Disruption of sequences in the knot region is known to prevent expression of functional holophytochrome, underscoring the functional significance of this unique structural motif (*4, 13–15*). Similarly, it has been reported that mutation of conserved GAF domain residues near the chromophore, including Tyr176, Asp207, and His260, profoundly influences assembly of apoprotein with bilin and/or photochemistry (*8, 11, 13, 14, 16–19*). This conserved knotted architecture and the conservation of key GAF domain residues are thus considered prerequisites for phytochrome photoconversion and signal transduction.

More distant relatives of phytochromes have been isolated which apparently do not possess this knotted structure. Members of the cyanobacterial Cph2 family lack the PAS domain, yet the N-terminal fragment of *Synechocystis* Cph2 exhibits red/far-red photoconversion (*8, 20*). This suggests that such photochemistry may occur in phytochrome-related GAF domains which lack the PAS/GAF knot. This is also the case for α-phycoerythrocyanin (α-PEC), which is structurally unrelated to phytochromes (*21, 22*). Proteins possessing only a phytochrome-related GAF domain have also been found in cyanobacteria (*23–30*); such proteins have been termed cyanobacteriochromes (*24, 31*) or phytochrome-related (Phr) proteins (*7*). Cyanobacteriochromes retain the conserved GAF domain Cys residue to which the bilin chromophore is covalently linked in plant phytochromes and in Cph1 (*8, 18, 32*) and also appear to possess a similar linkage between this residue and the bilin prosthetic group (*24, 29*).

The photochemical behavior of two cyanobacteriochromes has been characterized (*24, 28, 29, 31*): that of the blue light phototaxis regulator SyPixJ1/TaxD1 from *Synechocystis* sp. PCC 6803 (*sll0041* in the annotated genome), and that of the orthologous TePixJ protein from *Thermosynechococcus elongatus* (*tll0569* in the annotated genome). Both of these PixJ proteins exhibit a novel photoconversion between a P_b state, absorbing blue light with peak absorbance at 425−435 nm, and a P_g state, absorbing green light with a maximum at 531−535 nm. The P_b absorbance spectrum is thus similar to that of bilins with saturated C10 carbons, such as phycocyanorubin (Figure 1), while the P_g spectrum is reminiscent of the spectra of bilins with shortened conjugated systems, such as phycoerythrobilin or phycoviolobilin (PVB).

The current model for this blue/green photocycle is based on denaturation experiments. Using acidic urea as denaturant with the isolated GAF domain from TePixJ, Ikeuchi and coworkers demonstrated that P_b shifts to a much longer absorption maximum (∼594 nm (*31*)) upon denaturation. By contrast, P_g is apparently stable to acidic urea but can be converted to a comparable longer-wavelength species upon irradiation of the denatured holoprotein (*31*). The photochemical behavior of denatured TePixJ resembles that of denatured α-PEC, which utilizes a PVB chromophore and exhibits a photocycle at longer wavelengths (507 and 566 nm *21, 22*). Ikeuchi and colleagues have therefore proposed that TePixJ also harbors a PVB chromophore, which would absorb in the green region of the spectrum (*31*). The P_b state is proposed to arise from twisting a single ring (B or D) out of conjugation, such that the extended π system of the bilin is shortened and the chromophore absorbs at shorter wavelengths (*31*).

The present work was undertaken to characterize Tlr0924, a second representative of the five-member cyanobacteriochrome family encoded by the genome of *T. elongatus*. Through expression in bacteria engineered to synthesize PCB, we demonstrate that full-length Tlr0924, like PixJ, exhibits blue/green photoreversibility. By examining Tlr0924 spectra and photochemistry over a range of temperatures, we provide surprising new evidence that the P_g state is in thermal equilibrium with a previously unrecognized blue-absorbing state which can be spectrally and biochemically distinguished from the stable P_b species formed by irradiation of P_g with green light. Moreover, we show that the stable

blue-absorbing species is itself in equilibrium with a fourth state having peak absorbance at ~560 nm. Tlr0924 thus exhibits at least four spectroscopically distinct states. We also show that mutagenesis of Cys499, which is conserved in a subset of cyanobacteriochromes, ablates blue/green photoconversion of Tlr0924, resulting in formation of a red-absorbing adduct which exhibits no stable photoproducts. Our studies not only demonstrate that Cys499 is a key determinant for the blue/green switching properties of Tlr0924 but also provide new insight into the thermal and photochemical behavior of cyanobacteriochromes.

MATERIALS AND METHODS

Plasmid Construction. Cloning and mutagenesis were performed using *Escherichia coli* strain DH5α with standard techniques (*33, 34*). Genomic DNA from *T. elongatus* strain BP-1 (a generous gift of M. Ikeuchi, University of Tokyo) was used as template for polymerase chain reactions using appropriate primers to amplify the *tlr0924* gene and introduce *Bgl*II and *Xba*I sites at the 5′ and 3′ termini of the amplified sequence. The resulting product (2.3 kb) was cloned into the *Bgl*II and *Xba*I sites of pBAD-myc/hisB (Invitrogen) to yield pBAD-0924d. This expression construct introduced amino acids at the N-terminus (MDPSSRSEQLS...; extraneous amino acids underlined) as well as at the C-terminus (...RELSTLEQKLISEEDLNSAVDHHHHHH; extraneous amino acids underlined include the C-terminal myc and His_6 tags) for a total of 802 amino acids. Throughout, we use the numbering of the Tlr0924 protein as encoded by the *tlr0924* genomic sequence to designate residues in the recombinant Tlr0924 protein. Site-directed mutagenesis was performed using QuikChange XL (Stratagene) in accordance with the manufacturer's instructions. All sequences were confirmed by DNA sequencing.

Expression and Purification of Recombinant Proteins. Purified *Dr*BphP and $Y_{176}H$ Cph1 were the generous gifts of Keenan C. Taylor. Wild-type and mutant Tlr0924 proteins were expressed in *E. coli* strain LMG194 (Invitrogen) containing plasmid pPL-PCB (*35*) for production of PCB chromophore. Prior to expression, cells were grown overnight at 37 °C in minimal RM media containing 100 μg/mL ampicillin and 50 μg/mL kanamycin. Cells were diluted 1:250 into 50 mL of the same media and grown at 37 °C to an OD_{580} of ~0.5, then transferred into 500 mL of LB medium containing 100 μg/mL ampicillin plus 50 μg/mL kanamycin and 1 mM isopropyl-β-D-thiogalactopyranoside. After 1 h incubation at 37 °C, L-arabinose was added to a final concentration of 0.002% (w/v). Cultures were then incubated overnight at 25 °C and harvested at an OD_{580} of ~0.5. After harvesting by centrifugation (20 min at 4000*g* and 4 °C), cells were resuspended in 2−3 mL of ice-cold lysis buffer (50 mM Tris-HCl pH 7.0, 300 mM NaCl, 10% (v/v) glycerol, 0.2% (v/v) Tween 20, 1 mM 2-mercaptoethanol, and 20 mM imidazole) and lysed by passage through a French pressure cell (3 passes at 10,000 psi). Homogenates were clarified by ultracentrifugation (15 min at 200000*g* and 4 °C). Clarified lysates were applied onto Talon metal-affinity chromatography spin columns (1 mL bed volume, Clontech) that had been pre-equilibrated with 3 mL of lysis buffer. Columns were washed with 2 mL of lysis buffer, and His_6-tagged protein eluted with 1.2 mL of elution buffer (lysis buffer plus 200 mM imidazole). Eluates were dialyzed overnight at 4 °C in 500 mL of protein storage buffer (25 mM TES-KOH pH 7.5 containing 10% (v/v) glycerol), and purified protein was characterized immediately or flash-frozen in liquid nitrogen and stored at −80 °C.

Protein Chemistry. Protein samples were analyzed using SDS−PAGE with the Laemmli buffer system. Zinc-blot analysis was carried out as described previously (*36*). Purified Tlr0924 protein exhibited a positive signal in zinc blotting (Supplemental Figure 1, Supporting Information) and a mass/charge ratio consistent with a single attached PCB chromophore as measured by electrospray mass spectrometry (data not shown). Protein concentrations were determined using a modified Bradford assay (Bio-Rad) in accordance with the manufacturer's instructions using purified BSA (Sigma) as standard. BSA was calibrated with the reported extinction coefficient of BSA at 280 nm (*37*).

Homology Modeling and Bioinformatics. For homology modeling of the Tlr0924 GAF domain, alignments of this domain with the bilin-binding GAF domain of *Dr*BphP were prepared using MUSCLE (*38*) with or without manual editing. Alignments were used with the high-resolution structure of *Dr*BphP (PDB code 2O9C (*10*)) to generate apoprotein homology models using MODELER (*39*). These models were superposed with the *Dr*BphP structure, and the coordinates for the chromophore were then transferred to the homology models with a text editor. The resulting holoprotein models were manually edited in VMD (*40*) to reduce steric clashes and to improve geometry for attack of Cys527 at the $C3^1$ carbon. All structural figures were prepared using VMD, STRIDE, and Tachyon (*40–42*). Phylogenetic trees were generated in CLUSTAL (*43*) using the MUSCLE multiple sequence alignments.

Spectroscopy. Absorbance spectra were acquired on a Shimadzu UV-2401PC spectrophotometer or on a Cary 50 UV/vis spectrophotometer equipped with a temperature-controlled cuvette holder (Quantum Northwest) modified to permit irradiation of the sample from above to initiate photochemistry. Wild-type Tlr0924 was converted between P_b and P_g forms via irradiation from above in the Cary 50 using light from a 75 W xenon source passed through a water filter, bandpass interference filter (70 nm bandpass, 400 or 550 nm; CVI Laser), and liquid light guide (PTI). To test photochemistry of $C_{499}D$ mutant Tlr0924, protein was irradiated using a 650 nm interference filter (40 nm bandpass; CVI Laser) for 20 min, 10-fold longer than needed to drive wild-type Cph1 to photoequilibrium at the same optical density. Fluorescence spectra were acquired on a PTI QM-6/2005SE fluorimeter equipped with red-enhanced photomultiplier tubes. CD spectra were acquired on a Jasco J-720 spectropolarimeter at room temperature and are presented as the smoothed average of three scans with buffer subtraction.

Ab Initio Spectral Calculations. For Cph1 and Tlr0924, all calculations were performed on gas-phase model compounds mimicking the PCB adducts, but replacing the thioether linkage at $C3^1$ with a proton and replacing the propionate side chains with methyl groups. Starting geometries were constructed using MacMolPlt (*44*) and manual editing. Some geometries were preoptimized in GAMESS (*45*) at the AM1 level (*46, 47*) to confirm generation of a starting conformation that would permit convergence of the initial self-consistent field calculation. All geometries were

optimized at the RHF/6-31G* level followed by the B3LYP(VWN5)/6-31+G* level in Q-Chem or GAMESS, and TDDFT calculations of vertical excitation energies, oscillator strengths, and rotational strengths were performed at the BLYP/6-311+G* level of theory in Q-Chem or Gaussian03 (*45, 48, 49*). The 6-311+G* basis set was sufficient to give good convergence of the vertical excitation energy but was not sufficient for complete convergence of oscillator strength or rotational strength.

The lowest 15 excited states were calculated by TDDFT to give good coverage of both the red and blue absorbance bands of bilin chromophores. While TDDFT is known to give rise to artifacts in state ordering due to flaws in the description of excited states with charge-transfer character (*50*), we were able to identify excited states matching the red and blue/UV bands of the experimental absorbance spectra on the basis of calculated oscillator strengths and excitation energies. Most other peaks have very low oscillator strength, and thus the possibility remains that such weak transitions are actually present. Two transitions with significant oscillator strength were typically observed in between the red and blue bands; these are presumed to be charge-transfer states that are incorrectly ordered (*50*). One of these transitions had very weak calculated rotational strength, while the other had comparable rotational strength and sign to that of the transition considered the *bona fide* blue transition. Arguments based on the signs of CD spectra are therefore not affected by assignment of the blue band to either calculated transition, because the rotational signs are the same. A similar approach was attempted with a model compound mimicking the configuration and facial disposition of the BV-derived adduct of *Dr*BphP, but in this case multiple bands were predicted in the red region, making assignment equivocal. These bands had negative rotational strength, as is observed experimentally.

Bilin Nomenclature. We follow the designation of configuration about the methine bridges as *Z* or *E* (double bonds) and *syn* or *anti* (single bonds), as is standard (*51, 52*). In considering CD spectra of bilin chromophores and binding modes of bilins to the Tlr0924 GAF domain, we also found it useful to have a unique designation for the two faces of the bilin ring system, which is a less well-defined topic. The *M* and *P* nomenclature commonly used to designate helicity in cyclic configurations of bilins and verdins (*51*) could lead to confusion when applied to less helical configurations such as that found in α-PC (*53*), so we sought a simple, qualitative scheme applicable to the bilin configurations most relevant to available holoprotein crystal structures. We therefore use a modification of the proposed general convention for designating ring faces (*54*). In this scheme, the α face is taken as that face for which the ring atom numbering follows a clockwise direction, with the other face designated as β. Multiple ring systems would be given a common designation based on the lowest numbered ring (*54*).

However, for bilin chromophores, the lowest numbered ring (the A ring) adopts different geometries in the available crystal structures (*10, 53, 55*), which would imply that the face definitions for the rest of the molecule would also be variable. By contrast, available crystal structures of biliproteins exhibit the *Z,syn* configuration about C10 (*10, 53, 55, 56*), which implies that face definitions based on the B and C rings will be less variable and hence less confusing.

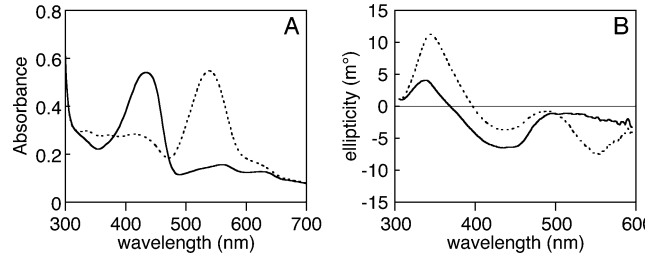

FIGURE 2: Spectroscopic characterization of Tlr0924 at room temperature. (A) Absorbance spectroscopy. Purified Tlr0924 exhibited peak absorbance at 434 nm (solid, P_b^S state). Irradiation of this peak resulted in a new peak wavelength of 538 nm (dashed, P_g). (B) CD spectroscopy. CD spectra were taken with Tlr0924 in the P_b^S (solid) or P_g (dashed) states. In both cases, the transition at lowest energy corresponded well to that observed in absorbance spectroscopy and exhibited negative rotation. Both states also exhibited second transitions (P_b^S, 336 nm; P_g, 344 nm) which exhibited positive rotation.

We therefore define the α and β faces of the bilin ring system based on the face definitions of the B ring. As shown in Supplemental Figure 2 (Supporting Information), these definitions are identical to those of the C ring for a *Z,syn* configuration about C10. In describing the disposition of the A or D rings relative to the B/C plane, we also add a subscript "f" to indicate the ring-face designation. When a ring is tilted but still partially coplanar with the B and C rings, we assign a facial disposition based on the position of the unique nitrogen atom (i.e., above or below the B/C plane). Using this convention, one can assign the dispositions of the A and D rings in the available phytochrome structures (*9–11*) as on the α face of the B/C ring system (Supplemental Figure 2). By contrast, the ring D nitrogen atom lies on the β face of the B/C ring system in both α-PC (*53*) and in the bilin-binding protein of *P. brassicae* (BBP (*56*)). We would thus designate BV in the *Dr*BphP structure as D-α_f ("D ring lying on the alpha face of the B and C rings") and both α-PC and BBP as D-β_f. Similarly, the conserved His260 and Asp207 of phytochromes lie on the bilin α and β faces, respectively (Supplemental Figure 2). It should be noted that this nomenclature is not well suited to twisted configurations about C10, regardless of whether they would formally be *Z,syn;* nor is it well suited to structures with a saturated C10 atom. In such cases, a more explicit description of the configuration would be required, for example by specification of the dihedral angles about the methine bridges. For the model compound geometries used in this work, such information is presented in Supplemental Table 1 (Supporting Information).

RESULTS

Tlr0924 Exhibits Blue/Green Photoconversion. We expressed recombinant full-length Tlr0924 protein with a C-terminal His_6 tag in *E. coli* cells harboring a second plasmid permitting production of the bilin chromophore PCB (*35*). The Tlr0924 protein was successfully purified as a holoprotein containing a single, covalently attached PCB chromophore as judged by zinc blot and mass spectrometry (Supplemental Figure 1 and data not shown). As was previously seen for PixJ proteins (*24, 28, 29*), the absorbance spectrum of Tlr0924 exhibited a peak at the edge of the visible region (434 nm, P_b: Figure 2A). Irradiation of Tlr0924

with 400 nm light resulted in a spectral shift to a longer wavelength (538 nm, P_g), which could then be efficiently converted back to P_b by irradiation with green light. At 25 °C, neither P_b nor P_g exhibited detectable fluorescence (data not shown). The P_b spectrum also exhibited a smaller peak at ~630 nm, which is visible in the P_b spectrum of PixJ proteins as well (*24, 28*). The relative size of this peak seemed to vary slightly between preparations, suggesting that it may be associated with an inactive or modified population of holoprotein.

The nonplanar conjugated π systems of bilins give rise to strong signals in CD spectroscopy. For example, the red band of Cph1 gives rise to a negative CD signal in the P_r state which changes to a positive signal in the P_{fr} state (*57*). The blue band of Cph1 exhibits a similar CD sign reversal upon photoconversion, but it is of opposite sign to the red band. In principle, CD spectroscopy can thus provide information about the conformation and configuration of a bilin chromophore, although microheterogeneity can have substantial effects on the observed spectra (*58*).

We examined the P_b and P_g states of Tlr0924 by CD spectroscopy (Figure 2B). Although the measuring beam caused significant photoconversion of P_g, the lowest-energy transition exhibited negative rotation in both cases. Moreover, the CD spectra were much less sensitive to interference from the 280 nm absorbance band of the protein, permitting unequivocal detection of the next highest transitions of the PCB chromophore (P_b, 336 nm; P_g, 344 nm). Both of these transitions exhibited positive rotation. The CD bands of Tlr0924 thus do not change sign upon photoconversion, unlike those of Cph1. A similar retention of CD sign upon photoconversion has been reported for the bacteriophytochrome Agp1 when assembled with the synthetic chromophore 18^1,18^2-dihydrobiliverdin (*59*).

Thermal Behavior of Tlr0924 in the Absence of Light. Our initial characterization of Tlr0924 was undertaken at room temperature. However, *T. elongatus* is a moderate thermophile which exhibits optimal growth at 55−60 °C (*60*). We therefore examined photoconversion over a range of temperatures. While Tlr0924 rapidly aggregated at 65 °C, blue/green photoconversion was readily observed between 5 and 55 °C (Figure 3A). The *in vivo* photosensory behavior of Tlr0924 and similar thermophilic cyanobacteriochromes is thus likely to be detection of blue and green light.

Photoconversion appeared less efficient at 5 °C, with a slight shift in the photochemical difference spectrum (Figure 3A). This was due to changes in the spectrum of the P_g state at this temperature. We therefore examined the behavior of P_g Tlr0924 as a function of temperature in the absence of light. Tlr0924 was cycled to the P_g state by irradiation with blue light at 40 °C and was then cooled to 20 °C in darkness. Absorbance spectra were taken until an apparent thermal equilibrium was established (<5 min), and the process was repeated after cooling to 10 °C and then to 5 °C (Scheme 1). The resulting equilibrium spectra show progressive appearance of a blue-absorbing species as temperature was lowered, with corresponding depletion of P_g and with isosbestic points at 363 and 456 nm (Figure 3B). Heating the sample from 5 to 20 °C resulted in rapid reversion to the previous 20 °C equilibrium spectrum (Supplemental Figure 3A, Supporting Information), demonstrating that these changes resulted from a reversible thermal equilibrium. The

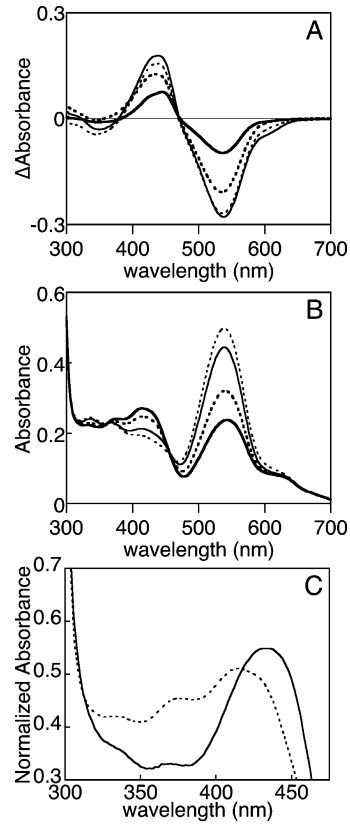

FIGURE 3: Photochemical and thermal equilibria of Tlr0924. (A) Tlr0924 was photoconverted between the P_b^S and P_g states at 20 °C (thin solid), 40 °C (thin dashed), 55 °C (thick dashed), and 5 °C (thick solid). Difference spectra are reported as ($P_b^S - P_g$). (B) Tlr0924 was driven to the P_g state at 40 °C (thin dashed). The sample was then progressively cooled to 20 °C (thin solid), 10 °C (thick dashed), and 5 °C (thick solid). At each temperature, the sample was incubated and spectra were taken until equilibrium was established. (C) Normalized absorbance spectra are presented for P_b^S (solid) and P_b^L (dashed) in the region of their peak wavelengths (P_b^S, 434 nm; P_b^L, 414 nm, 376 nm shoulder). The region at 335−350 nm contains P_b^S and P_g transitions (Figure 2B).

Scheme 1

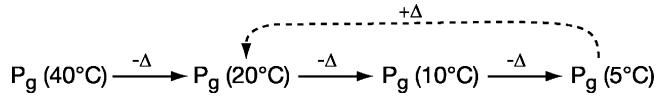

blue-absorbing species accumulated at low temperature was thus distinct from the P_b species generated by irradiation of P_g with green light, which did not convert to P_g in darkness at any temperature. We thus refer to the stable blue-absorbing P_b species produced by irradiation of P_g as P_b^S (stable blue-absorbing species) and the labile blue-absorbing species in thermal equilibrium with P_g as P_b^L (labile blue-absorbing species). These states could be distinguished spectroscopically as well as by their thermal behavior: P_b^S exhibited peak absorbance at 434 nm, while P_b^L exhibited peak absorbance at 414 nm with a pronounced shoulder at 376 nm (Figure 3C). The thermal difference spectrum for accumulation of P_b^L at 5 °C was also distinct from the photochemical difference spectrum at 5 °C, with a shorter peak wavelength in the blue region but with an identical trough wavelength in the green region (Figure 4A).

We also compared the spectra for the P_b^S state generated photochemically from P_g at different temperatures (Supplemental Figure 3C). At higher temperature, a small amount

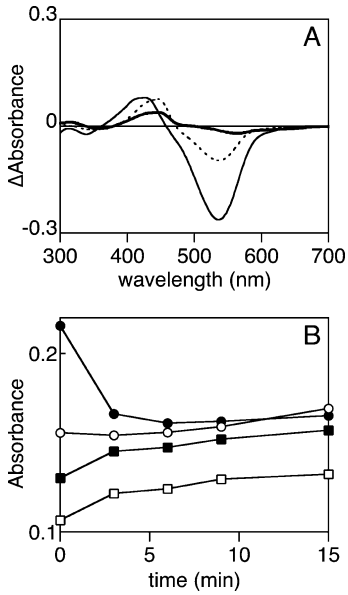

FIGURE 4: Characterization of the P_b^S and P_b^L states. (A) The photochemical difference spectrum at 5 °C (dashed, $P_b^S - P_g$) is compared with difference spectra for the thermal P_g/P_b^L equilibrium (thin solid, 40 °C to 5 °C) and the thermal P_b^S/P_g' equilibrium (thick solid, 20 °C to 40 °C). (B) Tlr0924 was cycled to the P_g state at 40 °C and then cooled to 5 °C to accumulate the P_b^L state. This sample was then irradiated with blue light. Changes in selected wavelengths are shown as a function of time, with full spectra presented in Supplemental Figure 3B (Supporting Information). Wavelengths are 540 nm (P_g, solid circles), 436 nm (P_b^S peak wavelength, hollow squares), 414 nm (P_b^L peak wavelength, solid squares), 336 nm (second transitions of P_b^S and P_g, hollow circles).

of a species with a longer peak wavelength (~560 nm) could be clearly seen, with a corresponding reduction in the P_b^S band and with isosbestic points at 338 and 498 nm. We designate this species as P_g'. However, the accumulation of this species at any temperature was much more modest than the accumulation of P_b^L at low temperature. This is clearly shown in Figure 4A, in which the 5 °C photochemical difference spectrum is compared with the thermal difference spectra for the P_b^L/P_g equilibrium and the P_b^S/P_g' equilibrium for a single sample. Moreover, photoconversion of Tlr0924 from P_b^S to P_g at 40 °C did not generate significantly lower amounts of P_g than at 20 °C (Figure 3A) despite the accumulation of P_g' relative to P_b^S at 40 °C (Supplemental Figure 3C). This suggests that the pool of P_g' present at 40 °C could be converted to P_g upon irradiation of P_b^S with blue light, implying that P_g' and P_b^S are in equilibrium. These experiments thus establish the existence of four spectroscopically and thermally distinct species within Tlr0924. Classical dark reversion (*thermal* conversion between *photochemical* states) could not be observed. The reported dark reversion of P_g at 4 °C in SyPixJ1 (*28*) may thus reflect slow equilibration of P_g to P_b^L.

The small amounts of P_g' that could be trapped precluded further direct characterization of this species. However, the substantial accumulation of P_b^L at low temperature permitted us to study its photochemistry by generating P_g at 40 °C, cooling the sample to shift the equilibrium toward the P_b^L state, and then irradiating with blue light and measuring absorbance spectra over time. Spectra from such an experiment are shown in Supplemental Figure 3B, with absorbance at selected wavelengths plotted as a function of time in Figure 4B. P_g is rapidly depleted upon irradiation with blue light, indicative of depletion of P_b^L and a further shift in the P_b^L/P_g equilibrium. The depletion of P_g at short times is accompanied by the expected increase in P_b^L and by similar changes at the peak wavelength for P_b^S, which may be caused by the spectral overlap of the two blue-absorbing states. Interestingly, P_g begins to reappear at later times. The region corresponding to the second transitions of P_b^S and P_g (Figure 2B) shows a slight depletion and a more rapid recovery. These results demonstrate that P_b^L is depleted by blue irradiation but do not permit unequivocal identification of a photoproduct.

Cys499 Is Essential for the Cyanobacteriochrome Photocycle. To learn more about the possible structural basis of blue/green photoconversion in Tlr0924 and PixJ, we generated homology models of the bilin-binding GAF domain of Tlr0924 based on the high-resolution crystal structure of the bacterial phytochrome *Dr*BphP (PDB accession 2O9C (*10*),). The underlying alignments of Tlr0924 and *Dr*BphP used to prepare homology models were generally unambiguous, but there was uncertainty in the region around the conserved Asp207-Ile208-Pro209 "DIP motif" of phytochromes (*Dr*BphP numbering), which can be aligned with Cys499-Phe500 of Tlr0924. We therefore used two possible alignments in this region (Supplemental Figure 4, Supporting Information) to prepare two different homology models for the Tlr0924 GAF domain (Supplemental Figure 5A, Supporting Information).

In the first alignment, these two sequence elements were aligned to each other (Supplemental Figure 4). The resulting structural model exhibited pronounced steric clashes between the bilin ring system and Phe500 of Tlr0924. Examination of this model revealed that these clashes could be alleviated were the bilin chromophore to be rotated approximately 180° about an axis between C5 and C15 (Supplemental Figure 5B). This rotation would not prevent covalent attachment of Cys527 to the bilin A ring. As a consequence of this rotation, Cys499 is placed in close proximity to C10 of the bilin chromophore (Supplemental Figure 5C).

In the second alignment, Cys499 was considered to reside in a small insertion in the region of the DIP motif (Supplemental Figure 4). In this case, the resulting model again placed Cys499 close to C10 of the bilin chromophore (Supplemental Figure 5C). Cys527 was again well positioned for covalent attachment to the $C3^1$ carbon of PCB. Cys499 is part of a larger DXCF motif that is conserved in a subclass of cyanobacteriochromes that includes both Tlr0924 and PixJ (see Discussion). Owing to the conservation of Cys499 and to its predicted location near the chromophore, we reasoned that Cys499 could be an important determinant for blue/green photoconversion and that mutagenesis of Cys499 would produce a different phenotype than mutagenesis of Cys527.

We tested this hypothesis by characterizing the $C_{527}A$ and $C_{499}A$ mutant proteins. Based on mutagenesis of SyPixJ1 (*28*), the $C_{527}A$ mutation is predicted to abolish the covalent linkage to the $C3^1$ carbon. The purified mutant protein indeed contained no detectable chromophore (Supplemental Figure 1), and the UV spectrum contained no absorbance bands beyond the 280 nm band of the aromatic amino acids (Supplemental Figure 6A, Supporting Information). In contrast, the $C_{499}A$ mutant protein could be expressed as a PCB adduct, but PCB incorporation was inefficient and the protein was prone to

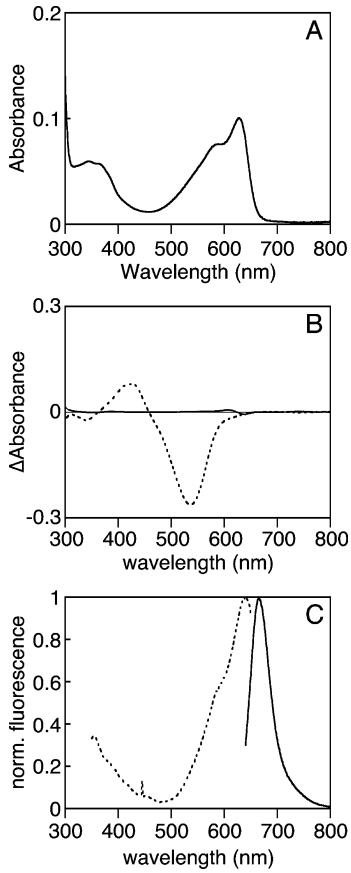

FIGURE 5: Characterization of C_{499}D mutant Tlr0924. (A) The absorbance spectrum of C_{499}D Tlr0924 at 20 °C exhibits peaks at 340 and 627 nm, with a shoulder at 583 nm. (B) Thermal difference spectra (5 °C to 40 °C) are shown for the wild-type P_g/P_b^L equilibrium (dashed) and for C_{499}D Tlr0924 (solid). (C) Normalized fluorescence spectra of C_{499}D Tlr0924. Excitation, dashed; emission, solid.

aggregation (data not shown). Its absorbance spectrum did not resemble that of wild-type Tlr0924, instead exhibiting a peak absorbance at approximately 630 nm (Supplemental Figure 6A). This result suggested that Cys499 was indeed important for the blue/green photocycle. However, the small amount of holoprotein that could be produced precluded further characterization of the C_{499}A mutant protein.

We therefore examined the C_{499}D mutant of Tlr0924, which replaces Cys499 with the Asp residue that might be equivalently positioned in phytochromes. In contrast to the C_{499}A and C_{527}A mutant proteins, C_{499}D Tlr0924 was expressed and purified as a PCB adduct with comparable incorporation of PCB to that of wild-type Tlr0924 (Supplemental Figure 1). Strikingly, the C_{499}D mutant protein exhibited a spectrum similar to that of the P_r form of Cph1, with two absorbance bands having λ_{max} of 627 and 345 nm and a shoulder at 583 nm (Figure 5A). This spectrum is blue-shifted relative to that for wild-type Cph1 and is more consistent with the spectrum reported for Y_{176}H Cph1, which exhibits red fluorescence and poor photoconversion (*16, 17*). Exhaustive red-light irradiation of C_{499}D mutant Tlr0924 failed to produce detectable changes in the spectrum (Supplemental Figure 6B), indicating that this mutant not only ablates formation of P_b^S but also prevents other long-lived photochemistry. Changes in temperature produced only slight changes in the absorbance spectrum of the mutant protein, which did not suggest the formation of spectrally distinct species (Figure 5B); indeed, the largest change was at very short wavelengths and could reflect changes in aromatic amino acids instead of changes in chromophore. As is also seen for the Y_{176}H mutant of Cph1, loss of photochemistry was accompanied by intense red fluorescence (Figure 5C). Comparison of the observed fluorescence of Y_{176}H Cph1 and C_{499}D Tlr0924 as a function of the observed absorbance (Supplemental Figure 6C) indicated that the fluorescence quantum yield of C_{499}D Tlr0924 was approximately 0.13, which is similar to that of Y_{176}H Cph1 (0.145 (*17*)). While photochemically compromised mutant phytochromes frequently exhibit spectra consistent with a cyclic configuration of chromophore, the relative intensity of the red and blue bands in the C_{499}D mutant and the shape of the red band are consistent with the presence of extended bilin (*17, 51*), suggesting that this protein contains a significant amount of PCB in an extended configuration similar to that of P_r phytochrome.

Assignment of the Chromophore Configuration in C_{499}D Tlr0924. As noted above, the electronic transitions of bilin chromophores are CD active. To learn more about the PCB configuration in the C_{499}D mutant protein, we compared the CD spectra of three proteins: the Tlr0924 C_{499}D mutant; the Y_{176}H mutant of Cph1, which is spectrally similar to P_r Cph1 and is photochemically similar to C_{499}D Tlr0924; and wild-type *Dr*BphP in the P_r state, which has a known chromophore configuration (*10*). As can be seen in Figure 6, all three proteins exhibit similar CD spectra, with only the peak wavelengths varying. Therefore, the chromophores in all three proteins adopt similar conformations as assayed by CD spectroscopy.

By contrast, both α-PC (the α-subunit of C-phycocyanin) and BBP (the bilin-binding protein from *P. brassicae)* exhibit CD spectra of opposite sign (*53, 56*). These proteins bind bilins in different configurations: PCB in α-PC adopts the C5-*Z,anti,* C10-*Z,syn,* C15-*Z,anti* configuration, while biliverdin IXγ adopts the cyclic C5-*Z,syn,* C10-*Z,syn,* C15-*Z,syn* configuration when bound to BBP and biliverdin IXα exhibits a C5-*Z,syn,* C10-*Z,syn,* C15-*Z,anti* configuration in the P_r state of *Dr*BphP (*10, 53, 56*). For BBP, which has a biliverdin IXγ chromophore bound in a cyclic configuration, the observed helicity in the crystal structure is in agreement with that predicted from the CD spectrum by symmetry (*56*). However, for other biliproteins, the different conformations and less symmetric chromophores make it difficult to interpret the CD spectra using such models (*51, 57*). Semiempirical results (*58*) suggest that *ab initio* techniques can provide useful insights into experimental bilin spectra.

To better elucidate the conformational features that determine CD spectra of PCB adducts, we calculated spectral parameters for model compounds using time-dependent density functional theory (TDDFT), which has recently been applied to various bilin systems (*61, 62*). We compared calculated results to the experimental spectra of both C_{499}D Tlr0924 and Y_{176}H Cph1, because we reasoned that a photochemically compromised mutant Cph1 would be less strongly dependent on the specific protein environment and would thus be better approximated by model compounds in the gas phase. Y_{176}H Cph1 should also be a more valid comparison to the photochemically compromised C_{499}D Tlr0924. The facial dispositions of the A and D rings (defined

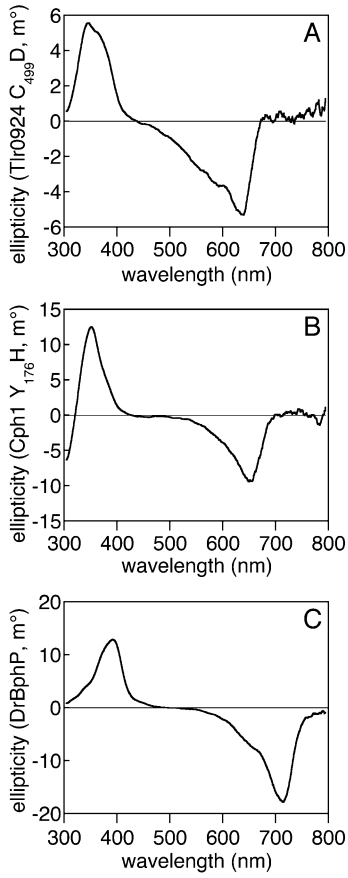

FIGURE 6: Comparison of the C_{499}D mutant of Tlr0924 with phytochromes by CD spectroscopy. (A) The CD spectrum of C_{499}D Tlr0924 (7.3 μM) exhibits negative rotation in the red absorbance band and positive rotation in the blue absorbance band. (B) The CD spectrum of Y_{176}H Cph1 (3.6 μM) exhibits similar features, as has been previously reported for wild-type Cph1 in the P_r state (*57*). (C) The CD spectrum of *Dr*BphP (4.4 μM) in the P_r state also exhibits similar features. All spectra are presented as the buffer-corrected, smoothed average of 3 scans at room temperature.

as in Supplemental Figure 2) were systematically varied, and both C5-*Z,syn* and C5-*Z,anti* configurations of PCB were evaluated. The dihedral angles about each methine bridge are reported in Supplemental Table 1 for all configurations tested in this study.

Varying the facial orientation of the D ring had a pronounced effect on the calculated CD spectrum (Table 1). When the D ring was α-facial, the red absorbance band of PCB was predicted to exhibit negative CD and the blue band was predicted to exhibit positive CD, as observed experimentally (Figure 6). This is in agreement with the observed D-α_f disposition of the BV adduct in *Dr*BphP (*10*). If instead the D ring were to be β-facial, the red band would be predicted to exhibit positive CD and the blue band negative CD (Table 1). The PCB chromophore in α-PC adopts such a disposition and exhibits such a spectrum (*53, 63*). By contrast, changing the configuration or facial disposition of the A ring did not produce changes in the sign of the CD spectrum (Table 1). These calculations thus demonstrate that the principal determinant for qualitative description of CD spectra in PCB adducts is the facial disposition of the D ring relative to the B/C ring system.

The calculated vertical excitation energies and rotations for the C5-*Z,syn* C10-*Z,syn* C15-*Z,anti* A-α_f D-α_f configuration are also in good agreement with the observed peak wavelengths of both Y_{176}H Cph1 and C_{499}D Tlr0924 (calculated λ_{max} 631 nm, negative; observed 627−635 nm, negative: Table 1 and Figure 6). This agreement is superior to that for alternative configurations (A-β_f, D-β_f, and/or C5-*Z,anti),* providing further evidence that the PCB in both of these photochemically compromised mutant proteins adopts such a geometry. Similarly good agreement was obtained for the configuration matching α-PC (calculated red λ_{max} 612 nm, positive; observed 618 nm, positive: Table 1). The combination of experimental spectroscopy and TDDFT calculations is consistent with assignment of the chromophore configuration in C_{499}D Tlr0924 as C5-*Z,syn* C10-*Z,syn* C15-*Z,anti*, with the A and D rings both lying on the α face of the B/C ring system. The PCB pocket in C_{499}D Tlr0924 thus closely resembles that of the P_r form of phytochrome.

DISCUSSION

We have characterized Tlr0924, a cyanobacteriochrome from *T. elongatus* which exhibits blue/green photoconversion rather than the characteristic red/far-red switching of phytochromes. These experiments utilize full-length Tlr0924 and include an examination of photochemistry at physiologically relevant temperatures for the thermophilic *T. elongatus* (*60*). Our studies reveal that the P_g state is in equilibrium with a previously uncharacterized P_b^L state, and we report the first CD spectra for a cyanobacteriochrome. We have also identified a Cys residue specifically implicated in blue/green photochemistry, because C_{499}D Tlr0924 is red-absorbing, fluorescent, and exhibits no readily detectable photochemistry. These results permit the development of a new model for the blue/green photocycle.

The current model for the cyanobacteriochrome photocycle, proposed by Ikeuchi and colleagues, was based on their pioneering characterization of PixJ (*31*). Their work demonstrated a striking resemblance between the absorbance spectra of the photoproducts of denatured PixJ and those of the photoproducts of denatured α-PEC, which uses phycoviolobilin (PVB) as chromophore (*21, 22, 31*). Based on these results, Ikeuchi and colleagues proposed a 2-state model (made explicit in Supplemental Figure 7A, Supporting Information) in which the PCB chromophore is isomerized to PVB upon binding to the apoprotein. P_b is proposed to arise from a structural deformation conferred by the protein, such that one ring twists out of conjugation and the spectrum is blue-shifted. Photoconversion of P_b to P_g would involve *Z*/*E* isomerization about the 15/16 bond, as in α-PEC (*21, 22*). The resulting 15*E* configuration would destabilize the blue-absorbing twisted structure, thereby relaxing the chromophore to give a green-absorbing 15*E* PVB (the P_g state). Excitation of P_g with green light would yield 15*Z* PVB, which would thermally convert to the twisted P_b state.

Formally, the proposed P_b state could arise via rotation about either the 9/10 bond (isolating ring B from rings C and D, Supplemental Figure 7A) or the 14/15 bond (isolating ring D from rings B and C, not shown). However, the latter alternative would remove the photochemically active 15/16 bond from the largest conjugated system. This would imply that the lowest-energy spectral transition in the blue would not be photochemically active. As the blue-absorbing transition is photochemically active, the P_b state would have to

Table 1: Calculated Spectral Parameters for Y_{176}H Cph1 and C_{499}D Tlr0924[a]

C5 configuration	facial disposition[b]	band	λ_{calc} (nm)	*f*	rotation	error (eV)
Z,syn	A-α_f D-α_f[c]	red	631	0.69	−	0.01
Z,syn	A-α_f D-α_f	blue	359	0.37	+	0.10
Z,syn	A-α_f D-β_f	red	638	0.62	+	0.02
Z,syn	A-α_f D-β_f	blue	356	0.43	−	0.10
Z,syn	A-β_f D-α_f	red	623	0.72	−	0.03
Z,syn	A-β_f D-α_f	blue	356	0.43	+	0.10
Z,syn	A-β_f D-β_f	red	627	0.61	+	0.01
Z,syn	A-β_f D-β_f	blue	360	0.37	−	0.10
Z,anti	A-α_f D-α_f	red	604	1.13	−	0.09
Z,anti	A-α_f D-α_f	blue	343	0.23	+	0.12
Z,anti	A-α_f D-β_f[d]	red	612	0.95	+	0.06
Z,anti	A-α_f D-β_f	blue	343	0.22	−	0.12
Z,anti	A-β_f D-α_f	red	603	1.16	−	0.09
Z,anti	A-β_f D-α_f	blue	344	0.15	+	0.11
Z,anti	A-β_f D-β_f	red	608	0.85	∼0	0.07
Z,anti	A-β_f D-β_f	blue	344	0.21	∼0	0.11

[a] Calculated for the blue (Soret) and red (*Q*) absorbance bands as described in Materials and Methods. λ_{calc}, peak wavelength; *f*, oscillator strength (linearly proportional to the integrated extinction coefficient); rotation, + or − for all transitions of rotational strength $>70 \times 10^{-40}$ erg-esu-cm/Gauss. Error is reported as the mean in electron volts relative to the observed peak wavelengths for Y_{176}H Cph1 (635 nm, 365 nm: (*17*)) and C_{499}D Tlr0924 (627 nm, 345 nm). Experimental uncertainty in the transition energy is 0.02 eV (red) and 0.2 eV (blue). [b] As defined in Materials and Methods and illustrated in Supplemental Figure 2. [c] Assigned to Y_{176}H Cph1 and C_{499}D Tlr0924 (this work). [d] Observed in α-PC (λ_{max} 618 nm, + rotation (*63*)). Error for α-PC is 0.02 eV.

arise via rotation of the B ring (Supplemental Figure 7A). The resulting chromophore would have one conjugated system comprising the C and D rings (also found in phycocyanorubin) and another system comprising the B ring in isolation (a monopyrrole). This model therefore predicts an absorbance band at ∼416−420 nm, by analogy to the absorbance spectra of phycocyanorubin and similar rubinoid species (*64–66*), and a series of bands at ∼170−215 nm, corresponding to the absorbance spectrum of pyrrole (*67*).

Although the UV spectra of PixJ and Tlr0924 are complex at wavelengths shorter than the 434 nm P_b^S peak, the CD spectrum of Tlr0924 provides good information about transitions in the 300−400 nm region (Figure 2B). The P_b^S spectrum displays the expected peak at 434 nm, with negative rotation, as well as a second peak at ∼336 nm which exhibits positive rotation. Upon photoconversion to P_g, both of these peaks are red-shifted without changes in rotational sign. The red-shift of both peaks upon photoconversion provides good evidence that both transitions are associated with the π system of the chromophore. Moreover, the value of ∼344 nm for the second transition of P_g is in good agreement with the transition at 341 nm measured for the P_g state of TePixJ by difference spectroscopy (*24*). These data thus demonstrate that P_b^S exhibits transitions at 434 nm and ∼336 nm. The 434 nm band is assigned to the lowest-energy transition of the C/D ring system. The 336 nm band is unlikely to arise from a higher-energy transition of the C/D ring system, because such a transition is absent in the spectra of rubins and of model dipyrrinones (*68*). This wavelength is also much longer than those observed for pyrrole (*67*) or protein residues. Therefore, the CD spectrum of native Tlr0924 in the P_b^S state is inconsistent with the presence of an isolated pyrrole ring. We thus conclude that native P_b^S does not possess a twisted PVB chromophore, indicating that the photochemical behavior of denatured PixJ is not a reliable indicator of the native chromophore structure for this state.

Based on the above arguments, there is a need to consider alternative structures for P_b^S. The peak wavelengths of Tlr0924 in the P_b^S state are strikingly similar to those of phycocyanorubin and similar adducts formed by dithionite treatment of phycocyanin (*64–66*). This would suggest an explanation for the vital role of Cys499 in the blue/green photocycle of Tlr0924: the thiol side chain of Cys499 could form a second covalent linkage to C10 of PCB, resulting in a rubinoid adduct (Figure 7). Such an adduct would be expected to exhibit peak absorbance at approximately 420 nm (*64–66*), with a second transition arising from the A and B rings and giving peak absorbance at ∼358−366 nm in the isolated chromophore (*66*). This shorter-wavelength transition would be further blue-shifted by the presence of the covalent linkage between Cys527 and the $C3^1$ carbon, explaining the 336 nm band of P_b^S. Similar adducts formed by thiol nucleophiles at the C10 atoms of model verdins or dihydrobilindiones have been described. Such species are thermally labile and facilitate *Z*/*E* photoisomerization at C15 (*64, 69*), implicating such photochemistry in cyanobacteriochromes as well. Light-driven *Z*/*E* isomerization of such a rubinoid species is also reminiscent of similar photochemistry in bilirubin, which forms the basis for phototherapeutic treatment of neonatal jaundice (*70, 71*).

The distinct behavior of P_b^S and P_b^L could therefore reflect a *Z*/*E* isomerization at C15. The protein matrix could stabilize the rubinoid adduct in the 15*Z* form (P_b^S), while photoisomerization to 15*E* could destabilize this linkage such that the rubinoid 15*E* P_b^L is in thermal equilibrium with a neutral PCB elimination product (Figure 7). Consistent with this hypothesis, neutral *ZZE* dihydrobilindiones have been reported to exhibit peak absorbance at wavelengths as short as 520 nm (*64*). The P_g species thus could be a neutral *ZZE* isomer of PCB without any further modification.

Photoconversion of P_b^S from 15*Z* to 15*E* could yield either P_b^L (if isomerization precedes elimination, Figure 7), a novel intermediate (if elimination precedes isomerization), or P_g itself (if the two processes are concerted). Photoconversion of P_b^L would be expected to give P_b^S, but the spectral overlap between these two states implies that the resulting P_b^S would then be converted to P_g by the same irradiation. The kinetic behavior of P_g upon irradiation of P_b^L (Figure 4B) could thus be viewed as a rapid decrease due to depletion of P_b^L by irradiation with blue light followed by a slower increase as

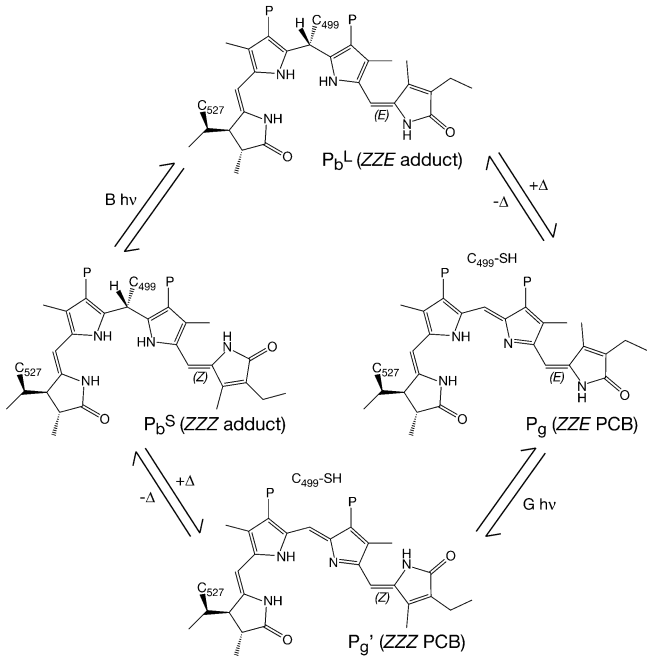

FIGURE 7: Proposed photocycle of Tlr0924. Tlr0924 assembles in the P_b^S state (middle left), in which the 15/16 bond is in the *Z* configuration and Cys499 forms a thioether linkage to the C10 carbon of the PCB chromophore. Irradiation of P_b^S with blue light results in formation of a photoequilibrium with P_b^L (top), in which the 15/16 bond is photoisomerized to the *E* configuration. P_b^L is in thermal equilibrium with P_g (middle right), in which Cys499 is eliminated to give neutral *ZZE* PCB. Irradiation of P_g with green light results in formation of a photoequilibrium with P_g' (bottom), in which the 15/16 bond is photoisomerized to the *Z* configuration. P_g' is in thermal equilibrium with P_b^S. All structures are drawn as C5-*Z,syn* C10-*Z,syn* 14/15 *anti* by analogy with the available crystal structures of phytochrome and with the C_{499}D mutant protein. However, the 14/15 bond could instead adopt the *syn* configuration favored in solution. The thioether linkage between Cys527 and the $C3^1$ carbon remains intact throughout the cycle. The stereochemistry at $C3^1$ is chosen by analogy to plant phytochrome (*32*), while the stereochemistry at C10 is that predicted by the "standard" homology model (Supplemental Figure 5). The "flipped" homology model predicts the opposite stereochemistry at C10.

P_b^S is generated and is itself photoconverted to P_g by the blue light source. Photoconversion of P_g with green light could generate the neutral 15*Z* PCB isomer P_g', and adduct formation at C10 would then generate P_b^S. Higher temperatures would disfavor formation of this linkage, explaining the modest accumulation of P_g' at 40 °C. At lower temperatures, the linkage between Cys499 and the 15*E* chromophore would be sufficiently stable to permit accumulation of the P_b^L 15*E* adduct (Figure 3B).

The role of Cys499 in this photocycle is thus quite different from the role of Cys527 and its equivalent Cys residues in phytochromes. The covalent linkage between Cys527 and $C3^1$ of the bilin chromophore is present in both phytochromes and cyanobacteriochromes, is essential for formation of Tlr0924 holoprotein (Supplemental Figure 1), and is not necessary for phytochrome photochemistry (*57, 72, 73*). By contrast, Cys499 is unique to a subset of cyanobacteriochromes (see below), is dispensable for formation of holoprotein, and is intimately associated with the blue/green photocycle. We therefore propose that the assembly of apoprotein with PCB to yield Tlr0924 holoprotein proceeds via formation of the covalent linkage between Cys527 and the $C3^1$ atom, with subsequent formation of the Cys499 adduct at C10. The presence of a minor red-absorbing component in both Tlr0924 (Figure 2A, Supplemental Figure 3C) and PixJ (*24*) could reflect variable oxidation of the thiol moiety of Cys499 or its equivalent in PixJ to cysteic acid, which would prevent efficient adduct formation and favor protonation of the chromophore. Protonation of the chromophore would explain the red-shift of this *ZZZ* species relative to the neutral P_g'.

While this hypothesis explains the observed photochemical/thermal behaviors of Tlr0924 and the importance of Cys499, there are alternative models. For example, Cys499 could be involved in reducing PCB to phycocyanorubin to produce P_b^S. Photoconversion to P_g could then proceed via a combination of *Z*/*E* isomerization at C15 and a tautomerization at C10 and C4 to give 2,3-dihydrophycoviolobilin (Supplemental Figure 7B). In such a model, Cys499 would function as a proton transfer catalyst rather than as a nucleophile. One could also envision a model in which Cys499 acts as a nucleophile, but the site of the second linkage migrates between C10 and C4, with the latter linkage corresponding to a violinoid P_g species (Supplemental Figure 7C). While adduct formation at C4 has been reported for linear tetrapyrroles (*74*), this position is sterically crowded and such attack by a bulky thiol nucleophile would seem unlikely. Based on the available data for both cyanobacteriochromes and model compounds, we favor the model presented in Figure 7, in which formation of the thiol adduct is reversible.

Several experimental approaches should prove useful in testing this hypothesis, which is currently based on the absorbance and CD spectra for wild-type Tlr0924 and on the phenotypes of the mutant Tlr0924 proteins lacking Cys499. The classical test of denaturation would in principle distinguish between a saturated C10 position and a twisted C10 geometry that interrupts conjugation. However, as discussed above, denaturation of PixJ under acidic conditions apparently does not preserve the chemical structure of P_b^S. Treatment with neutral urea has been reported to preserve the P_b spectrum of PixJ (*29*), but the same does not hold true for treatment with SDS (*31*). In the case of Tlr0924, the presence of additional domains in the protein and the low efficiency of holoprotein formation (Supplemental Figure 1) make it difficult to assess the efficacy of such agents in unfolding the protein. Characterization of the Tlr0924 GAF domain alone could permit not only such experiments but also techniques such as derivatization of free Cys side chains. Our understanding of the cyanobacteriochrome photocycle will ultimately benefit most from crystallographic studies.

We predict that those cyanobacteriochrome GAF domains containing equivalents to Cys499 will exhibit blue/green photoswitching. This Cys is only present in a subset of cyanobacteriochrome GAF domains, while the Cys residue responsible for ligation to the bilin A ring (Cys527 in Tlr0924) is much more widespread. Cyanobacteriochromes which contain a Cys equivalent to Cys527 of Tlr0924 can be separated into three classes based on the sequence aligned to the phytochrome DIP motif (Supplemental Figure 8, Supporting Information): class I, which includes the first cyanobacteriochromes to be discovered, PlpA and RcaE (*25, 27*); class II, which comprises proteins with the conserved DXCF motif containing Cys499, such as PixJ and

Tlr0924; and class III, which has a third consensus sequence in this region and which has not yet been biochemically or functionally characterized. This subset definition is consistent with classification based on phylogenetic analysis of the entire GAF domain (Supplemental Figure 8), suggesting that it is likely to serve as a valid criterion for inferring the presence of blue/green photochemistry. Interestingly, the C-terminal GAF domain of *Synechocystis* Cph2 is classified as a class II cyanobacteriochrome by sequence (Supplemental Figure 8). While photochemistry has not been reported for this domain, it is known to exhibit an absorbance spectrum consistent with P_b^S (*8*). Moreover, *Synechocystis* Cph2 has been implicated in blue light signaling (*75*). Whether it is possible for class I or class III cyanobacteriochromes to exhibit similar blue/green photochemistry in the absence of an equivalent Cys is not yet known, though we would predict that they should instead exhibit some other photochemical behavior.

Functional information is available for the class I cyanobacteriochromes PlpA, CikA, and RcaE (*25–27, 76*); however, these proteins are diverged from the class II cyanobacteriochromes such as Tlr0924. In *Synechocystis,* both PixJ and Cph2 contain class II cyanobacteriochrome GAF domains (Supplemental Figure 7), and functional evidence implicates both proteins in blue light phototaxis (*23, 30, 75*). Less is known about the biological functions of other cyanobacteriochromes, but it seems plausible that the class II cyanobacteriochrome GAF domain functions as a blue/green photosensory module that can interact with a variety of signaling output domains, as do the red/far-red photosensory modules of phytochromes. Depending upon the precise coupling of the photosensory input domain to the signaling outputs, the photo and thermal equilibria between P_b^S, P_b^L, and P_g might also enable cyanobacteriochromes to assay the light and temperature environments simultaneously. In Tlr0924, the CBS domains N-terminal to the GAF domain suggest that the activity of this protein might be regulated by ATP or similar molecules (*77*), while the presence of a GGDEF domain suggests that Tlr0924 may be a diguanylyl cyclase (*78*). Tlr0924 may thus be able to integrate a variety of signals (ATP/AMP level, redox effects on Cys499, bilin production from heme, temperature, and light) in generating the cyclic-di-GMP second messenger, reminiscent of the integration of light and metabolic signals by phytochromes.

ACKNOWLEDGMENT

We are indebted to Prof. Masahiko Ikeuchi (University of Tokyo) for the gift of *T. elongatus* genomic DNA and to Prof. Julie Leary (U. C. Davis) for analysis of purified Tlr0924 by mass spectrometry. We thank Prof. Richard Vierstra (U. of Wisconsin-Madison) for the original *Dr*BphP expression construct, Keenan C. Taylor for the generous gift of purified Y_{176}H Cph1 and *Dr*BphP, and Prof. Stephanie Dungan (Dept. of Food Science, U. C. Davis) for use of the Jasco CD spectrometer. We thank Alison Breen, Melissa Lucey, Clea Lopez, Brittany Ashlock, Kathy Marshall, Amanda Yeaton-Massey, Nova Szoka and Lea Dunn (all from Mills College) for technical assistance, Amanda J. Fischer and Abigail Y. Jang (U. C. Davis) for assistance with the early stages of this project. We are indebted to Shara Compton (U. C. Davis) for instruction on the Jasco CD spectrometer.

SUPPORTING INFORMATION AVAILABLE

8 figures and 1 table. This material is available free of charge via the Internet at http://pubs.acs.org.

REFERENCES

1. Briggs, W. R., and Spudich, J. A., Eds. (2005) *Handbook of Photosensory Receptors*, Wiley VCH, Weinheim.
2. Schäfer, E., and Nagy, F., Eds. (2005) *Photomorphogenesis in Plants and Bacteria: Function and Signal Transduction Mechanisms*, 3rd ed., Springer, Dordrecht, The Netherlands.
3. Montgomery, B. L., and Lagarias, J. C. (2002) Phytochrome ancestry. Sensors of bilins and light. *Trends Plant Sci. 7*, 357–366.
4. Karniol, B., Wagner, J. R., Walker, J. M., and Vierstra, R. D. (2005) Phylogenetic analysis of the phytochrome superfamily reveals distinct microbial subfamilies of photoreceptors. *Biochem. J. 392*, 103–116.
5. Gärtner, W., and Braslavsky, S. E. (2003) The phytochromes: Spectroscopy and function, in *Photoreceptors and Light Signalling* (Batschauer, A., Ed.) pp 136−180, Royal Society of Chemistry, Cambridge, U.K.
6. Yeh, K.-C., Wu, S.-H., Murphy, J. T., and Lagarias, J. C. (1997) A cyanobacterial phytochrome two-component light sensory system. *Science 277*, 1505–1508.
7. Rockwell, N. C., Su, Y. S., and Lagarias, J. C. (2006) Phytochrome structure and signaling mechanisms. *Annu. Rev. Plant Biol. 57*, 837–858.
8. Wu, S. H., and Lagarias, J. C. (2000) Defining the bilin lyase domain: Lessons from the extended phytochrome superfamily. *Biochemistry 39*, 13487–13495.
9. Wagner, J. R., Brunzelle, J. S., Forest, K. T., and Vierstra, R. D. (2005) A light-sensing knot revealed by the structure of the chromophore binding domain of phytochrome. *Nature 438*, 325–331.
10. Wagner, J. R., Zhang, J., Brunzelle, J. S., Vierstra, R. D., and Forest, K. T. (2007) High resolution structure of Deinococcus bacteriophytochrome yields new insights into phytochrome architecture and evolution. *J. Biol. Chem. 282*, 12298–12309.
11. Yang, X., Stojkovic, E. A., Kuk, J., and Moffat, K. (2007) Crystal structure of the chromophore binding domain of an unusual bacteriophytochrome, RpBphP3, reveals residues that modulate photoconversion. *Proc. Natl. Acad. Sci. USA 104*, 12571–12576.
12. Rockwell, N. C., and Lagarias, J. C. (2006) The structure of phytochrome. A picture is worth a thousand spectra. *Plant Cell 18*, 4–14.
13. Bhoo, S. H., Hirano, T., Jeong, H. Y., Lee, J. G., Furuya, M., and Song, P. S. (1997) Phytochrome photochromism probed by site-directed mutations and chromophore esterification. *J. Am. Chem. Soc. 119*, 11717–11718.
14. Wagner, J. R., Zhang, J., von Stetten, D., Gunther, M., Murgida, D. H., Mroginski, M. A., Walker, J. M., Forest, K. T., Hildebrandt, P., and Vierstra, R. D. (2008) Mutational Analysis of Deinococcus radiodurans Bacteriophytochrome Reveals Key Amino Acids Necessary for the Photochromicity and Proton Exchange Cycle of Phytochromes. *J. Biol. Chem. 283*, 12212–12226.
15. Zhao, K. H., Ran, Y., Li, M., Sun, Y. N., Zhou, M., Storf, M., Kupka, M., Böhm, S., Bubenzer, C., and Scheer, H. (2004) Photochromic biliproteins from the cyanobacterium Anabaena sp. PCC 7120: lyase activities, chromophore exchange, and photochromism in phytochrome AphA. *Biochemistry 43*, 11576–11588.
16. Fischer, A. J., and Lagarias, J. C. (2004) Harnessing phytochrome's glowing potential. *Proc. Natl. Acad. Sci. U.S.A. 101*, 17334–17339.
17. Fischer, A. J., Rockwell, N. C., Jang, A. Y., Ernst, L. A., Waggoner, A. S., Duan, Y., Lei, H., and Lagarias, J. C. (2005) Multiple roles of a conserved GAF domain tyrosine residue in cyanobacterial and plant phytochromes. *Biochemistry 44*, 15203–15215.
18. Hahn, J., Strauss, H. M., Landgraf, F. T., Gimenez, H. F., Lochnit, G., Schmieder, P., and Hughes, J. (2006) Probing protein-chromophore interactions in Cph1 phytochrome by mutagenesis. *FEBS J. 273*, 1415–1429.
19. von Stetten, D., Seibeck, S., Michael, N., Scheerer, P., Mroginski, M. A., Murgida, D. H., Krauss, N., Heyn, M. P., Hildebrandt, P., Borucki, B., and Lamparter, T. (2007) Highly conserved residues

Asp-197 and His-250 in Agp1 phytochrome control the proton affinity of the chromophore and Pfr formation. *J. Biol. Chem. 282*, 2116–2123.
20. Park, C. M., Kim, J. I., Yang, S. S., Kang, J. G., Kang, J. H., Shim, J. Y., Chung, Y. H., Park, Y. M., and Song, P. S. (2000) A second photochromic bacteriophytochrome from Synechocystis sp PCC 6803: Spectral analysis and down-regulation by light. *Biochemistry 39*, 10840–10847.
21. Zhao, K. H., Haessner, R., Cmiel, E., and Scheer, H. (1995) Type I reversible photochemistry of phycoerythrocyanin involves Z/E-isomerization of alpha-84 phycoviolobilin chromophore. *Biochim. Biophys. Acta Bioenerg. 1228*, 235–243.
22. Zhao, K. H., and Scheer, H. (1995) Type I and type II reversible photochemistry of phycoerythrocyanin alpha-subunit from Mastigocladus laminosus both involve Z, E isomerization of phycoviolobilin chromophore and are controlled by sulfhydryls in apoprotein. *Biochim. Biophys. Acta Bioenerg. 1228*, 244–253.
23. Bhaya, D., Takahashi, A., and Grossman, A. R. (2001) Light regulation of type IV pilus-dependent motility by chemosensor-like elements in Synechocystis PCC6803. *Proc. Natl. Acad. Sci. U.S.A. 98*, 7540–7545.
24. Ishizuka, T., Shimada, T., Okajima, K., Yoshihara, S., Ochiai, Y., Katayama, M., and Ikeuchi, M. (2006) Characterization of cyanobacteriochrome TePixJ from a thermophilic cyanobacterium Thermosynechococcus elongatus strain BP-1. *Plant Cell Physiol. 47*, 1251–1261.
25. Kehoe, D. M., and Grossman, A. R. (1996) Similarity of a chromatic adaptation sensor to phytochrome and ethylene receptors. *Science 273*, 1409–1412.
26. Schmitz, O., Katayama, M., Williams, S. B., Kondo, T., and Golden, S. S. (2000) CikA, a bacteriophytochrome that resets the cyanobacterial circadian clock. *Science 289*, 765–768.
27. Wilde, A., Churin, Y., Schubert, H., and Borner, T. (1997) Disruption of a Synechocystis sp. PCC 6803 gene with partial similarity to phytochrome genes alters growth under changing light qualities. *FEBS Lett. 406*, 89–92.
28. Yoshihara, S., Katayama, M., Geng, X., and Ikeuchi, M. (2004) Cyanobacterial phytochrome-like PixJ1 holoprotein shows novel reversible photoconversion between blue- and green-absorbing forms. *Plant Cell Physiol. 45*, 1729–1737.
29. Yoshihara, S., Shimada, T., Matsuoka, D., Zikihara, K., Kohchi, T., and Tokutomi, S. (2006) Reconstitution of blue-green reversible photoconversion of a cyanobacterial photoreceptor, PixJ1, in phycocyanobilin-producing. *Escherichia coli. Biochemistry 45*, 3775–3784.
30. Yoshihara, S., Suzuki, F., Fujita, H., Geng, X. X., and Ikeuchi, M. (2000) Novel putative photoreceptor and regulatory genes required for the positive phototactic movement of the unicellular motile cyanobacterium Synechocystis sp PCC 6803. *Plant Cell Physiol. 41*, 1299–1304.
31. Ishizuka, T., Narikawa, R., Kohchi, T., Katayama, M., and Ikeuchi, M. (2007) Cyanobacteriochrome TePixJ of Thermosynechococcus elongatus harbors phycoviolobilin as a chromophore. *Plant Cell Physiol. 48*, 1385–1390.
32. Lagarias, J. C., and Rapoport, H. (1980) Chromopeptides from phytochrome. The structure and linkage of the Pr form of the phytochrome chromophore. *J. Am. Chem. Soc. 102*, 4821–4828.
33. Ausubel, F. M. (1994) *Current Protocols in Molecular Biology*, John Wiley & Sons, New York, 4 vols. (loose-leaf).
34. Sambrook, J., Fritsch, E. F., and Maniatis, T. (1989) *Molecular Cloning: A Laboratory Manual*, 2nd ed., Cold Spring Harbor Laboratory Press, New York.
35. Gambetta, G. A., and Lagarias, J. C. (2001) Genetic engineering of phytochrome biosynthesis in bacteria. *Proc. Natl. Acad. Sci. U.S.A. 98*, 10566–10571.
36. Berkelman, T. R., and Lagarias, J. C. (1986) Visualization of bilin-linked peptides and proteins in polyacrylamide gels. *Anal. Biochem. 156*, 194–201.
37. Scopes, R. K. (1974) Measurement of protein by spectrophotometry at 205 nm. *Anal. Biochem. 59*, 277–282.
38. Edgar, R. C. (2004) MUSCLE: multiple sequence alignment with high accuracy and high throughput. *Nucleic Acids Res. 32*, 1792–1797.
39. Fiser, A., and Sali, A. (2003) Modeller: generation and refinement of homology-based protein structure models. *Methods Enzymol. 374*, 461–491.
40. Humphrey, W., Dalke, A., and Schulten, K. (1996) VMD: visual molecular dynamics. *J. Mol. Graphics 14*, 33–38.
41. Frishman, D., and Argos, P. (1995) Knowledge-based protein secondary structure assignment. *Proteins 23*, 566–579.
42. Stone, J. (1998) *An Efficient Library for Parallel Ray Tracing and Animation*, Thesis, University of Missouri-Rolla.
43. Higgins, D. G., Thompson, J. D., and Gibson, T. J. (1996) Using CLUSTAL for multiple sequence alignments. *Methods Enzymol. 266*, 383–402.
44. Bode, B. M., and Gordon, M. S. (1998) MacMolPlt: a graphical user interface for GAMESS. *J. Mol. Graphics Modell. 16*, 133–138, 164.
45. Schmidt, M. W., Baldridge, K. K., Boatz, J. A., Elbert, S. T., Gordon, M. S., Jensen, J. H., Koseki, S., Matsunaga, N., Nguyen, K. A., Su, S., Windus, T. L., Dupuis, M., and Montgomery, J. A., Jr. (1993) General atomic and molecular electronic structure system. *J. Comput. Chem. 14*, 1347–1363.
46. Dewar, M. J. S., and Yuan, Y. C. (1990) AM1 parameters for sulfur. *Inorg. Chem. 29*, 3881–3890.
47. Dewar, M. J. S., Zoebisch, E. G., Healy, E. F., and Stewart, J. J. P. (1985) Development and use of quantum mechanical molecular models. 76. AM1: a new general purpose quantum mechanical molecular model. *J. Am. Chem. Soc. 107*, 3902–3909.
48. Frisch, M. J., Trucks, G. W., Schlegel, H. B., Scuseria, G. E., Robb, M. A., Cheeseman, J. R., Montgomery, J. J. A., Vreven, T., Kudin, K. N., Burant, J. C., Millam, J. M., Iyengar, S. S., Tomasi, J., Barone, V., Mennucci, B., Cossi, M., Scalmani, G., Rega, N., Petersson, G. A., Nakatsuji, H., Hada, M., Ehara, M., Toyota, K., Fukuda, R., Hasegawa, J., Ishida, M., Nakajima, T., Honda, Y., Kitao, O., Nakai, H., Klene, M., Li, X., Knox, J. E., Hratchian, H. P., Cross, J. B., Bakken, V., Adamo, C., Jaramillo, J., Gomperts, R., Stratmann, R. E., Yazyev, O., Austin, A. J., Cammi, R., Pomelli, C., Ochterski, J. W., Ayala, P. Y., Morokuma, K., Voth, G. A., Salvador, P., Dannenberg, J. J., Zakrzewski, V. G., Dapprich, S., Daniels, A. D., Strain, M. C., Farkas, O., Malick, D. K., Rabuck, A. D., Raghavachari, K., Foresman, J. B., Ortiz, J. V., Cui, Q., Baboul, A. G., Clifford, S., Cioslowski, J., Stefanov, B. B., Liu, G., Liashenko, A., Piskorz, P., Komaromi, I., Martin, R. L., Fox, D. J., Keith, T., AlLaham, M. A., Peng, C. Y., Nanayakkara, A., Challacombe, M., Gill, P. M. W., Johnson, B., Chen, W., Wong, M. W., Gonzalez, C., and Pople, J. A. (2004), *Gaussian 03, Revision D.01*, Gaussian, Inc., Wallingford, CT.
49. Shao, Y., Molnar, L. F., Jung, Y., Kussmann, J., Ochsenfeld, C., Brown, S. T., Gilbert, A. T., Slipchenko, L. V., Levchenko, S. V., O'Neill, D. P., DiStasio, R. A., Jr., Lochan, R. C., Wang, T., Beran, G. J., Besley, N. A., Herbert, J. M., Lin, C. Y., VanVoorhis, T., Chien, S. H., Sodt, A., Steele, R. P., Rassolov, V. A., Maslen, P. E., Korambath, P. P., Adamson, R. D., Austin, B., Baker, J., Byrd, E. F., Dachsel, H., Doerksen, R. J., Dreuw, A., Dunietz, B. D., Dutoi, A. D., Furlani, T. R., Gwaltney, S. R., Heyden, A., Hirata, S., Hsu, C. P., Kedziora, G., Khalliulin, R. Z., Klunzinger, P., Lee, A. M., Lee, M. S., Liang, W., Lotan, I., Nair, N., Peters, B., Proynov, E. I., Pieniazek, P. A., Rhee, Y. M., Ritchie, J., Rosta, E., Sherrill, C. D., Simmonett, A. C., Subotnik, J. E., Woodcock, H. L., 3rd, Zhang, W., Bell, A. T., Chakraborty, A. K., Chipman, D. M., Keil, F. J., Warshel, A., Hehre, W. J., Schaefer, H. F., 3rd, Kong, J., Krylov, A. I., Gill, P. M., and Head-Gordon, M. (2006) Advances in methods and algorithms in a modern quantum chemistry program package. *Phys. Chem. Chem. Phys. 8*, 3172–3191.
50. Dreuw, A., and Head-Gordon, M. (2005) Single-reference ab initio methods for the calculation of excited states of large molecules. *Chem. Rev. 105*, 4009–4037.
51. Falk, H. (1989) *The Chemistry of Linear Oligopyrroles and Bile Pigments*, Springer-Verlag, Vienna, 621 pp.
52. Moss, G. P. (1987) Nomenclature of Tetrapyrroles (Recommendations 1986) IUPAC-IUB Joint Commission on Biochemical Nomenclature. *Pure Appl. Chem. 59*, 779–832.
53. Duerring, M., Schmidt, G. B., and Huber, R. (1991) Isolation, crystallization, crystal structure analysis and refinement of constitutive C-phycocyanin from the chromatically adapting cyanobacterium *Fremyella diplosiphon* at 1.66 Å resolution. *J. Mol. Biol. 217*, 577–592.
54. Rose, I. A., Hanson, K. R., Wilkinson, K. D., and Wimmer, M. J. (1980) A suggestion for naming faces of ring compounds. *Proc. Natl. Acad. Sci. U.S.A. 77*, 2439–2441.
55. Duerring, M., Huber, R., Bode, W., Ruembeli, R., and Zuber, H. (1990) Refined 3-dimensional structure of phycoerythrocyanin from the cyanobacterium Mastigocladus laminosus at 2.7-Å. *J. Mol. Biol. 211*, 633–644.

56. Huber, R., Schneider, M., Mayr, I., Muller, R., Deutzmann, R., Suter, F., Zuber, H., Falk, H., and Kayser, H. (1987) Molecular structure of the bilin binding protein (BBP) from Pieris brassicae after refinement at 2.0 Å resolution. *J. Mol. Biol. 198*, 499–513.
57. Borucki, B., Otto, H., Rottwinkel, G., Hughes, J., Heyn, M. P., and Lamparter, T. (2003) Mechanism of Cph1 phytochrome assembly from stopped-flow kinetics and circular dichroism. *Biochemistry 42*, 13684–13697.
58. Scharnagl, C., and Schneider, S. (1989) UV-visible absorption and circular dichroism spectra of the subunits of C-phycocyanin I: quantitative assessment of the effect of chromophore-protein interactions in the a-subunit. *J. Photochem. Photobiol. B 3*, 603–614.
59. Seibeck, S., Borucki, B., Otto, H., Inomata, K., Khawn, H., Kinoshita, H., Michael, N., Lamparter, T., and Heyn, M. P. (2007) Locked 5Zs-biliverdin blocks the Meta-Ra to Meta-Rc transition in the functional cycle of bacteriophytochrome Agp1. *FEBS Lett. 581*, 5425–5429.
60. Yamaoka, T., Satoh, K., and Katoh, S. (1978) Photosynthetic activities of a thermophilic blue-green alga. *Plant Cell Physiol. 19*, 943–954.
61. Borg, O. A., and Durbeej, B. (2007) Relative ground and excited-state pKa values of phytochromobilin in the photoactivation of phytochrome: a computational study. *J. Phys. Chem. B 111*, 11554–11565.
62. Zazza, C., Sanna, N., and Aschi, M. (2007) Theoretical study of alpha-84 phycocyanobilin chromophore from the thermophilic cyanobacterium Synechococcus elongatus. *J. Phys. Chem. B 111*, 5596–5601.
63. Mimuro, M., Füglistaller, P., Rümbeli, R., and Zuber, H. (1986) Functional assignment of chromophores and energy transfer in C phycocyanin isolated from the thermophilic cyanobacterium Mastigocladus laminosus. *Biochim. Biophys. Acta 848*, 155–166.
64. Kufer, W., Cmiel, E., Thuemmler, F., Ruediger, W., Schneider, S., and Scheer, H. (1982) Studies on plant bile pigments. II. Regioselective photochemical and acid catalyzed *Z,E* isomerization of dihydrobilindione as phytochrome model. *Photochem. Photobiol. 36*, 603–607.
65. Kufer, W., and Scheer, H. (1982) Rubins and rubinoid addition products from phycocyanin. *Z. Naturforsch. 37c*, 179–192.
66. Terry, M. J., Maines, M. D., and Lagarias, J. C. (1993) Inactivation of phytochrome- and phycobiliprotein-chromophore precursors by rat liver biliverdin reductase. *J. Biol. Chem. 268*, 26099–26106.
67. Palmer, M. H., Walker, I. C., and Guest, M. F. (1998) The electronic states of pyrrole studied by optical (VUV) absorption, near-threshold electron energy-loss (EEL) spectroscopy and ab initio multi-reference configuration interaction calculations. *Chem. Phys. 238*, 179–199.
68. Byun, Y.-S., and Lightner, D. A. (1991) Exciton coupling from dipyrrinone chromophores. *J. Org. Chem. 56*, 6027–6033.
69. Falk, H., Mueller, N., and Schlederer, T. (1980) Beitrage zur Chemie der Pyrrolpigmente, 35. Mitt.: Eine regioselektive, reversible Addition an Bilatriene-abc. *Monatsh. Chem. 111*, 159–175.
70. Lamola, A. A., Blumberg, W. E., McClead, R., and Fanaroff, A. (1981) Photoisomerized bilirubin in blood from infants receiving phototherapy. *Proc. Natl. Acad. Sci. U.S.A. 78*, 1882–1886.
71. McDonagh, A. F., Palma, L. A., and Lightner, D. A. (1980) Blue light and bilirubin excretion. *Science 208*, 145–151.
72. Jorissen, H. J., Quest, B., Lindner, I., Tandeau de Marsac, N., and Gartner, W. (2002) Phytochromes with noncovalently bound chromophores: the ability of apophytochromes to direct tetrapyrrole photoisomerization. *Photochem. Photobiol. 75*, 554–559.
73. Lamparter, T., and Michael, N. (2005) Agrobacterium phytochrome as an enzyme for the production of ZZE bilins. *Biochemistry 44*, 8461–8469.
74. Falk, H., and Zrunek, U. (1984) Beitrage zur Chemie der Pyrrolpigmente, 52 Mitt.: Phytochrommodelstudien: Eine reversible Addition an Δ-4 von 2,3-dihydrobilatrienen-abc. *Monatsh. Chem. 115*, 101–111.
75. Wilde, A., Fiedler, B., and Börner, T. (2002) The cyanobacterial phytochrome Cph2 inhibits phototaxis towards blue light. *Mol. Microbiol. 44*, 981–988.
76. Terauchi, K., Montgomery, B. L., Grossman, A. R., Lagarias, J. C., and Kehoe, D. M. (2004) RcaE is a complementary chromatic adaptation photoreceptor required for green and red light responsiveness. *Mol. Microbiol. 51*, 567–577.
77. Meyer, S., Savaresi, S., Forster, I. C., and Dutzler, R. (2007) Nucleotide recognition by the cytoplasmic domain of the human chloride transporter ClC-5. *Nat. Struct. Mol. Biol. 14*, 60–67.
78. Ryjenkov, D. A., Tarutina, M., Moskvin, O. V., and Gomelsky, M. (2005) Cyclic diguanylate is a ubiquitous signaling molecule in bacteria: insights into biochemistry of the GGDEF protein domain. *J. Bacteriol. 187*, 1792–1798.
79. Jung, L. J., Chan, C. F., and Glazer, A. N. (1995) Candidate genes for the phycoerythrocyanin alpha subunit lyase. Biochemical analysis of pecE and pecF interposon mutants. *J. Biol. Chem. 270*, 12877–12884.
80. Zhao, K. H., Deng, M. G., Zheng, M., Zhou, M., Parbel, A., Storf, M., Meyer, M., Strohmann, B., and Scheer, H. (2000) Novel activity of a phycobiliprotein lyase: both the attachment of phycocyanobilin and the isomerization to phycoviolobilin are catalyzed by the proteins PecE and PecF encoded by the phycoerythrocyanin operon. *FEBS Lett. 469*, 9–13.

BI800088T